Supplement of Quantifying black carbon light absorption enhancement by a novel statistical approach

Cheng Wu[1,2], Dui Wu[1,2,3], Jian Zhen Yu[4,5,6]

[1] Institute of Mass Spectrometer and Atmospheric Environment, Jinan University, Guangzhou 510632, China

[2] Guangdong Provincial Engineering Research Center for on-line source apportionment system of air pollution, Guangzhou 510632, China

[3] Institute of Tropical and Marine Meteorology, China Meteorological Administration, Guangzhou 510080, China

[4] Division of Environment, Hong Kong University of Science and Technology, Clear Water Bay, Hong Kong, China

[5] Atmospheric Research Centre, Fok Ying Tung Graduate School, Hong Kong University of Science and Technology, Nansha, China

[6] Department of Chemistry, Hong Kong University of Science and Technology, Clear Water Bay, Hong Kong, China

Corresponding to: Cheng Wu (wucheng.vip@foxmail.com) and Jian Zhen Yu (jian.yu@ust.hk)

This SI contains five tables and nineteen figures.

Uncertainty of E_{abs} estimation

The uncertainty of E_{abs} estimation depends on uncertainty propagation from MAE uncertainty, which can be calculated from (Harris, 2010):

$$MAE_{Unc} = MAE \times \sqrt{\left(\frac{\sigma_{abs,Unc}}{\sigma_{abs}}\right)^2 + \left(\frac{EC_{Unc}}{EC}\right)^2} \quad \text{S1}$$

$$E_{abs,Unc} = E_{abs} \times \sqrt{\left(\frac{MAE_{Unc}}{MAE}\right)^2 + \left(\frac{MAE_{p,Unc}}{MAE_p}\right)^2} \quad \text{S2}$$

Descriptions of customized programs used in this study for data analysis and visualization

Several computer programs were developed to meet specific research purpose in this study. All the programs are based on Igor Pro (www.wavemetrics.com) that provides a friendly GUI. Brief descriptions are given below.

MRS program (Igor Pro based)

The program (Figure S15) is written in Igro Pro (WaveMetrics, Inc. Lake Oswego, OR, USA) to feasible MRS calculation via a user-friendly GUI. The MRS application is not limited in SOC estimation, but can also be extended to other applications (e.g. E_{abs} estimation) as long as a reliable tracer is available.

MRS calculation can be done by different temporal cycles (batch calculation): by year, by year&season, by season, by year&month, by month, by year&month&hour. Data filter is also available to calculate MRS on a specific subset of data.

The program is available from https://sites.google.com/site/wuchengust.

Mie program and source code written in Igor Pro

A computer program (Figure S16) written in Igro Pro (WaveMetrics, Inc. Lake Oswego, OR, USA) for Mie scattering calculation. Both BHMIE and BHCOAT (coated particles) algorithms(Bohren and Huffman, 1983) are included. The program is also capable of batch calculation for both algorithms. Available from https://sites.google.com/site/wuchengust.

Aethalometer data processing program (Igor Pro based)

This handy tool (Figure S17) can perform different corrections (e.g. Weingartner, Virkkula) on Aethalometer data. Raw Aethalometer data suffers from several artifacts including filter matrix effect (multiple scattering), loading effect (shadowing) and scattering effect. Careful corrections are needed for reporting light absorption coefficient from attenuation measurement. This Igor based program can directly import Aethalometer raw data and perform corrections (algorithm can be selected by user). Results can be exported to .csv files. Extra information including statistics of sensor voltage from each channel, sampling flow rate, etc are plotted for a quick QA/QC check. Available from https://sites.google.com/site/wuchengust.

Histbox program (Igor Pro based)

A handy tool (Figure S18) to generate histogram and box plots with many powerful features. Data can be sorted by different time scale and batch plotting is available. Available from https://sites.google.com/site/wuchengust.

Scatter plot program

Scatter plot (Figure S19) is a handy tool to maximize the efficiency of data visualization in atmospheric science. The program includes Deming, WODR and York algorithm for linear regression, which consider uncertainties in both X and Y, that is more realistic for atmospheric applications. It is Igor based, and packed with lots of useful features for data analysis and graph plotting, including batch plotting, data masking via GUI, color coding in Z axis, data filtering and grouping. Available from https://sites.google.com/site/wuchengust.

Reference

Andreae, M. O., Schmid, O., Yang, H., Chand, D., Yu, J. Z., Zeng, L. M., and Zhang, Y. H.: Optical properties and chemical composition of the atmospheric aerosol in urban Guangzhou, China, Atmos. Environ., 42, 6335-6350, doi: 10.1016/j.atmosenv.2008.01.030, 2008.

Bohren, C. F. and Huffman, D. R.: Absorption and scattering of light by small particles, Wiley, New York, xiv, 530 p. pp., 1983.

Chan, T. W., Brook, J. R., Smallwood, G. J., and Lu, G.: Time-resolved measurements of black carbon light absorption enhancement in urban and near-urban locations of southern Ontario, Canada, Atmos. Chem. Phys., 11, 10407-10432, 2011.

Chow, J. C., Watson, J. G., Doraiswamy, P., Chen, L. W. A., Sodeman, D. A., Lowenthal, D. H., Park, K., Arnott, W. P., and Motallebi, N.: Aerosol light absorption, black carbon, and elemental carbon at the Fresno Supersite, California, Atmos Res, 93, 874-887, doi: DOI 10.1016/j.atmosres.2009.04.010, 2009.

Chuang, P. Y., Duvall, R. M., Bae, M. S., Jefferson, A., Schauer, J. J., Yang, H., Yu, J. Z., and Kim, J.: Observations of elemental carbon and absorption during ACE-Asia and implications for aerosol radiative properties and climate forcing, J. Geophys. Res., 108, 8634, doi: Doi 10.1029/2002jd003254, 2003.

Doran, J. C., Barnard, J. C., Arnott, W. P., Cary, R., Coulter, R., Fast, J. D., Kassianov, E. I., Kleinman, L., Laulainen, N. S., Martin, T., Paredes-Miranda, G., Pekour, M. S., Shaw, W. J., Smith, D. F., Springston, S. R., and Yu, X. Y.: The T1-T2 study: evolution of aerosol properties downwind of Mexico City, Atmos. Chem. Phys., 7, 1585-1598, doi: 10.5194/acp-7-1585-2007, 2007.

Harris, D. C.: Quantitative chemical analysis, 8th ed., W.H. Freeman and Co., New York, 2010.

Knox, A., Evans, G. J., Brook, J. R., Yao, X., Jeong, C. H., Godri, K. J., Sabaliauskas, K., and Slowik, J. G.: Mass Absorption Cross-Section of Ambient Black Carbon Aerosol in Relation to Chemical Age, Aerosol. Sci. Technol., 43, 522-532, doi: Doi 10.1080/02786820902777207, 2009.

Lack, D. A. and Cappa, C. D.: Impact of brown and clear carbon on light absorption enhancement, single scatter albedo and absorption wavelength dependence of black carbon, Atmos. Chem. Phys., 10, 4207-4220, doi: DOI 10.5194/acp-10-4207-2010, 2010.

Lan, Z.-J., Huang, X.-F., Yu, K.-Y., Sun, T.-L., Zeng, L.-W., and Hu, M.: Light absorption of black carbon aerosol and its enhancement by mixing state in an urban atmosphere in South China, Atmos. Environ., 69, 118-123, doi: http://dx.doi.org/10.1016/j.atmosenv.2012.12.009, 2013.

Liu, D., Flynn, M., Gysel, M., Targino, A., Crawford, I., Bower, K., Choularton, T., Jurányi, Z., Steinbacher, M., Hüglin, C., Curtius, J., Kampus, M., Petzold, A., Weingartner, E., Baltensperger, U., and Coe, H.: Single particle characterization of black carbon aerosols at a tropospheric alpine site in Switzerland, Atmos. Chem. Phys., 10, 7389-7407, doi: 10.5194/acp-10-7389-2010, 2010.

Mayol-Bracero, O. L., Gabriel, R., Andreae, M. O., Kirchstetter, T. W., Novakov, T., Ogren, J., Sheridan, P., and Streets, D. G.: Carbonaceous aerosols over the Indian Ocean during the Indian Ocean Experiment (INDOEX): Chemical characterization, optical properties, and probable sources, J. Geophys. Res., 107, 8030, doi: Doi 10.1029/2000jd000039, 2002.

Moosmuller, H., Chakrabarty, R. K., Ehlers, K. M., and Arnott, W. P.: Absorption Angstrom coefficient, brown carbon, and aerosols: basic concepts, bulk matter, and spherical particles, Atmos. Chem. Phys., 11, 1217-1225, doi: DOI 10.5194/acp-11-1217-2011, 2011.

Pandolfi, M., Cusack, M., Alastuey, A., and Querol, X.: Variability of aerosol optical properties in the Western Mediterranean Basin, Atmos. Chem. Phys., 11, 8189-8203, doi: DOI 10.5194/acp-11-8189-2011, 2011.

Thompson, J. E., Hayes, P. L., Jimenez, K. A. J. L., Zhang, X., Liu, J., Weber, R. J., and Buseck, P. R.: Aerosol Optical Properties at Pasadena, CA During CalNex 2010, Atmos Environ, doi: 10.1016/j.atmosenv.2012.03.011, 2012.

Wang, Q., Huang, R., Zhao, Z., Cao, J., Ni, H., Tie, X., Zhu, C., Shen, Z., Wang, M., and Dai, W.: Effects of photochemical oxidation on the mixing state and light absorption of black carbon in the urban atmosphere of China, Environmental Research Letters, 12, 044012, 2017.

Wang, Q. Y., Huang, R. J., Cao, J. J., Han, Y. M., Wang, G. H., Li, G. H., Wang, Y. C., Dai, W. T., Zhang, R. J., and Zhou, Y. Q.: Mixing State of Black Carbon Aerosol in a Heavily Polluted Urban Area of China: Implications for Light Absorption Enhancement, Aerosol. Sci. Technol., 48, 689-697, doi: 10.1080/02786826.2014.917758, 2014.

Xu, J., Bergin, M. H., Yu, X., Liu, G., Zhao, J., Carrico, C. M., and Baumann, K.: Measurement of aerosol chemical, physical and radiative properties in the Yangtze delta region of China, Atmos. Environ., 36, 161-173, 2002.

Yang, M., Howell, S. G., Zhuang, J., and Huebert, B. J.: Attribution of aerosol light absorption to black carbon, brown carbon, and dust in China - interpretations of atmospheric measurements during EAST-AIRE, Atmos. Chem. Phys., 9, 2035-2050, 2009.

Table S1. Comparison of Mass absorption efficiency (MAE) at various locations. For literature MAE values at different wavelengths rather than 550nm, an estimated MAE_{550} is given in the brackets following equations given by Moosmuller et al. (2011) assuming AAE of 1.

Location	Type	Sampling Duration	Inlet	λ (nm)	σ_{abs} Instrument	EC determination protocol	σ_{abs} ±1 S.D. (Mm^{-1})	EC mass ($\mu g\ m^{-3}$)	estimated MAE_p* ($m^2\ g^{-1}$)	observed MAE ($m^2\ g^{-1}$) arithmetic mean ±1 S.D.	observed MAE ($m^2\ g^{-1}$) Gaussian fit	Reference
Guangzhou, China	Suburban	2012.2-2013.1	$PM_{2.5}$	550	AE	NIOSH_TOT	42.20±29.41	2.63±2.27	13*	19.02±6.60	16.16	This study
Shenzhen, China	Urban	2011.8-9	$PM_{2.5}$	532	PAS	LII	25.4±19.0	4.0±3.1	/	6.5±0.5[6.29±0.48]	/	(Lan et al., 2013)
Xi'an, China	Urban	2012.12-2013.1	$PM_{2.5}$	870	PAS	LII	/	8.8±7.3	7.17[11.34]	/	7.62[12.05]	(Wang et al., 2014)
Xi'an, China	Urban	2013.2	$PM_{2.5}$	532	PAS	LII				14.6±5.6	12.7	(Wang et al., 2017)
Guangzhou, China	Urban	2004.10	$PM_{2.5}$	532	PAS	NIOSH_TOT	91±60	7.1	7.7[7.44]	/	/	(Andreae et al., 2008)
Fresno, USA	Urban	2005.8-9	$PM_{2.5}$	532	PAS	IMPROVE_A_TOR	5.06	1.01	/	6.1±2.5[5.9±2.42]	/	(Chow et al., 2009)
						NIOSH_TOT		0.58	/	9.3±2.4[8.99±2.32]	/	
T1,Mexico city, Mexico	Suburban	2006.3	$PM_{2.5}$	870	PAS	NIOSH_TOT	/	/	/	9.2~9.7***[14.55~15.34]	/	(Doran et al., 2007)
Pasadena, USA	Urban	2010.5-6	$PM_{2.5}$	532	AM	NIOSH_TOT	3.8±3.4	0.6~0.7	5.7[5.51]	/	/	(Thompson et al., 2012)
Toronto, Canada	Urban	2006.12-2007.1	$PM_{2.5}$	760	PAS	NIOSH_TOT	/	/	6.9~9.1** [9.53~12.57]	9.3~9.9[12.85~13.68]	/	(Knox et al., 2009)
Toronto, Canada	Suburban						3~6	0.10~0.14	/	30~43[42.6~61.06]	/	
Windsor, Canada	Urban	2007.8	$PM_{2.5}$	781	PAS	LII	4.4±2.9	0.27±0.23	/	16±1[22.72±1.42]	/	(Chan et al., 2011)
Ottawa, Canada	Urban						26±17	1.7±0.9	/	15±3[21.3±4.26]	/	
Beijing, China	Rural	2005.3	/	550	AE	NIOSH_TOT	/	/	9.5	11.3	/	(Yang et al., 2009)
Montseny, Spin	Rural (Mediterranean)	2009.11-2010.10	PM_{10}	637	MAAP	NIOSH_TOT	2.8±2.2	/	10.4[12.04]	/	/	(Pandolfi et al., 2011)
Jungfraujoch, Switzerland	Rural (high alpine)	2007.2-3	/	637	MAAP	LII	/	/	/	10.2±3.2[11.81±3.71]	/	(Liu et al., 2010)
Lin'an, China	Rural	1999.11	$PM_{2.5}$	550	PSAP	NIOSH_TOT	23±14	3.4±1.7	/	8.6±7.0	/	(Xu et al., 2002)
Jeju Island, Korea	Coastal Rural, (East China Sea)	2001.4	PM_{10}	550	PSAP	NIOSH_TOT	/	/	/	12.6±2.6	/	(Chuang et al., 2003)
Maldives	Oceanic rural	1999.2-3	PM_3	550	PSAP	EGA	62±34	2.5±1.4	6.6	8.1	/	(Mayol-Bracero et al., 2002)

*Determined by Minimium R Squared method; ** Median values;

AE:Aethalometer ; PAS photo acoustic spectrometer; MAAP: Multi Angle Absorption Photometer; PSAP: particle soot absorption photometer; AM: albedo meter; LII: Laser induced incandescence

Table S2. Statistics of monthly MAE_{550nm}

Month	95th	75th	50th	25th	5th	Mean	Max	Min	S.D.	N
Feb-2012	31.29	22.04	18.12	15.74	13.90	19.72	47.73	8.50	5.78	533
Mar-2012	28.33	19.80	17.48	15.92	13.77	18.78	45.56	10.98	4.92	663
Apr-2012	33.06	22.66	18.24	16.11	13.85	20.21	48.29	6.01	6.23	595
May-2012	33.74	23.35	19.61	17.17	14.73	21.22	48.40	6.33	5.99	533
Jun-2012	39.73	27.17	21.76	18.72	15.04	23.70	49.07	5.62	7.37	333
Jul-2012	35.96	24.62	19.12	15.64	12.71	21.14	49.63	9.23	7.65	609
Aug-2012	42.94	27.99	22.01	16.24	12.55	23.50	49.95	9.75	8.98	556
Sep-2012	33.15	21.11	17.61	15.25	12.99	19.31	49.54	10.39	6.18	684
Oct-2012	20.72	15.84	13.95	12.60	11.18	14.70	34.09	7.34	3.21	715
Nov-2012	28.64	18.67	15.53	13.72	11.95	17.18	48.41	8.34	5.58	506
Dec-2012	29.92	19.32	15.74	13.67	11.78	17.39	48.73	9.33	5.86	591
Jan-2013	21.60	16.24	14.48	13.03	11.79	15.33	48.48	7.16	3.97	709

Table S3. Statistics of monthly $AAE_{470-660}$

Month	95th	75th	50th	25th	5th	Mean	Max	Min	S.D.	N
Feb-2012	1.41	1.25	1.17	1.09	0.94	1.17	1.70	0.78	0.14	533
Mar-2012	1.31	1.17	1.08	1.00	0.92	1.09	1.45	0.68	0.12	663
Apr-2012	1.16	1.07	1.01	0.95	0.83	1.00	1.35	0.56	0.10	587
May-2012	1.11	1.03	0.99	0.93	0.85	0.98	1.21	0.50	0.09	530
Jun-2012	1.17	1.09	1.03	0.97	0.88	1.02	1.29	0.39	0.10	333
Jul-2012	1.19	1.09	1.03	0.97	0.84	1.03	1.38	0.47	0.11	604
Aug-2012	1.16	1.08	1.03	0.97	0.88	1.02	1.30	0.64	0.08	556
Sep-2012	1.21	1.11	1.04	0.98	0.90	1.05	1.37	0.68	0.10	684
Oct-2012	1.25	1.15	1.07	1.01	0.93	1.08	1.36	0.84	0.10	715
Nov-2012	1.22	1.14	1.09	1.03	0.97	1.09	1.45	0.88	0.08	506
Dec-2012	1.31	1.21	1.15	1.09	0.99	1.15	1.41	0.92	0.09	591
Jan-2013	1.36	1.25	1.17	1.11	1.00	1.18	1.63	0.90	0.11	709

Table S4. Statistics of monthly SSA

Month	95th	75th	50th	25th	5th	Mean	Max	Min	S.D.	N
Feb-2012	0.91	0.89	0.87	0.84	0.79	0.86	0.94	0.65	0.04	530
Mar-2012	0.91	0.89	0.86	0.83	0.77	0.85	0.95	0.42	0.05	660
Apr-2012	0.92	0.89	0.86	0.83	0.76	0.85	0.94	0.45	0.06	552
May-2012	0.92	0.90	0.87	0.83	0.74	0.85	0.94	0.45	0.06	532
Jun-2012	0.92	0.89	0.86	0.81	0.74	0.85	0.95	0.64	0.06	328
Jul-2012	0.91	0.87	0.83	0.79	0.71	0.83	0.95	0.57	0.06	602
Aug-2012	0.94	0.92	0.89	0.85	0.79	0.88	0.96	0.67	0.05	547
Sep-2012	0.94	0.91	0.88	0.84	0.75	0.87	0.96	0.55	0.06	682
Oct-2012	0.94	0.93	0.91	0.89	0.84	0.90	0.96	0.66	0.03	715
Nov-2012	0.91	0.89	0.87	0.83	0.75	0.85	0.94	0.18	0.06	506
Dec-2012	0.91	0.89	0.86	0.82	0.74	0.85	0.94	0.66	0.05	591
Jan-2013	0.91	0.89	0.87	0.85	0.79	0.86	0.93	0.64	0.04	709

Table S5. Statistics of monthly E_{abs550}

Month	95th	75th	50th	25th	5th	Mean	Max	Min	S.D.	N
Feb-2012	2.24	1.57	1.29	1.12	0.99	1.41	3.41	0.61	0.41	533
Mar-2012	1.76	1.23	1.09	0.99	0.86	1.17	2.83	0.68	0.31	663
Apr-2012	2.45	1.68	1.35	1.19	1.03	1.50	3.58	0.44	0.46	595
May-2012	2.50	1.73	1.45	1.27	1.09	1.57	3.58	0.47	0.44	533
Jun-2012	2.74	1.87	1.50	1.29	1.04	1.63	3.38	0.39	0.51	333
Jul-2012	2.95	2.02	1.57	1.28	1.04	1.73	4.07	0.76	0.63	609
Aug-2012	3.61	2.35	1.85	1.36	1.05	1.97	4.20	0.82	0.75	556
Sep-2012	2.53	1.61	1.34	1.16	0.99	1.47	3.78	0.79	0.47	684
Oct-2012	1.87	1.43	1.26	1.14	1.01	1.32	3.07	0.66	0.29	715
Nov-2012	2.31	1.51	1.25	1.11	0.96	1.39	3.90	0.67	0.45	506
Dec-2012	2.54	1.64	1.33	1.16	1.00	1.47	4.13	0.79	0.50	591
Jan-2013	1.83	1.38	1.23	1.10	1.00	1.30	4.11	0.61	0.34	709

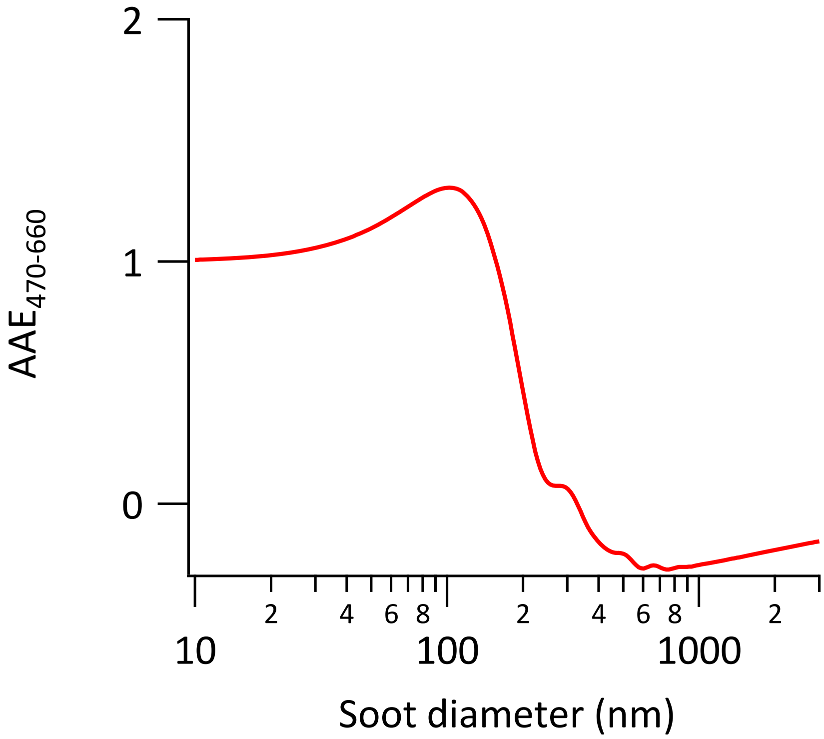

Figure S1. Mie simulated $AAE_{470\text{-}660}$ of a bare soot particle as a function of diameter with a Refractive index of 1.85 – 0.71i.

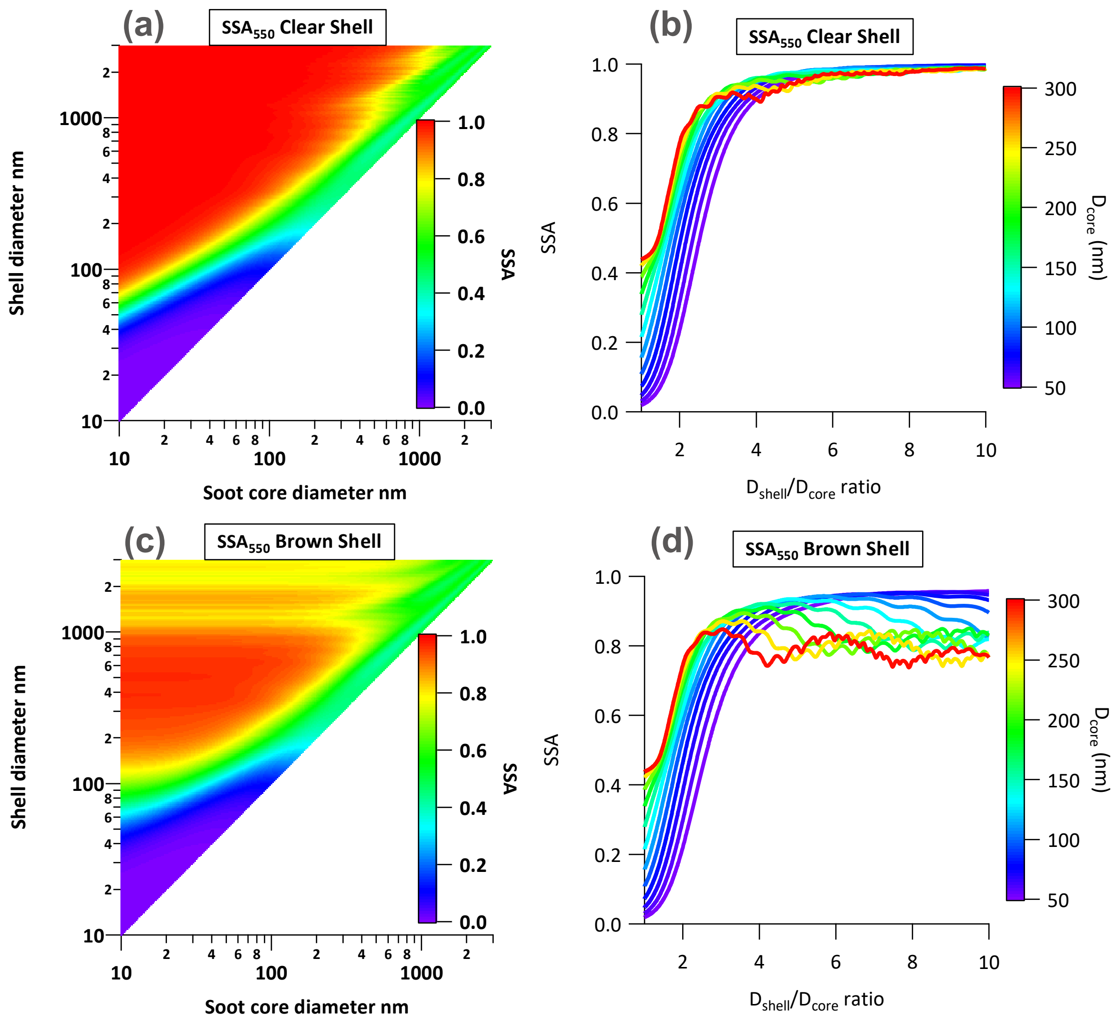

Figure S2. Mie simulated size dependency of soot particles SSA at wavelength 550 nm. (a)Combination of different shell (y axis) and core diameters (x axis). The color coding represents the SSA of a particle with specific core and shell size; (b) Cross-sections views of (a). The color coding represents different D_{core} in the range of 50 – 300 nm. (c)Combination of different shell (y axis) and core diameters (x axis). The color coding represents the E_{abs} of a particle with specific core and shell size; (d) Cross-sections views of (c). The color coding represents different diameters of soot core in the range of 50 – 300 nm.

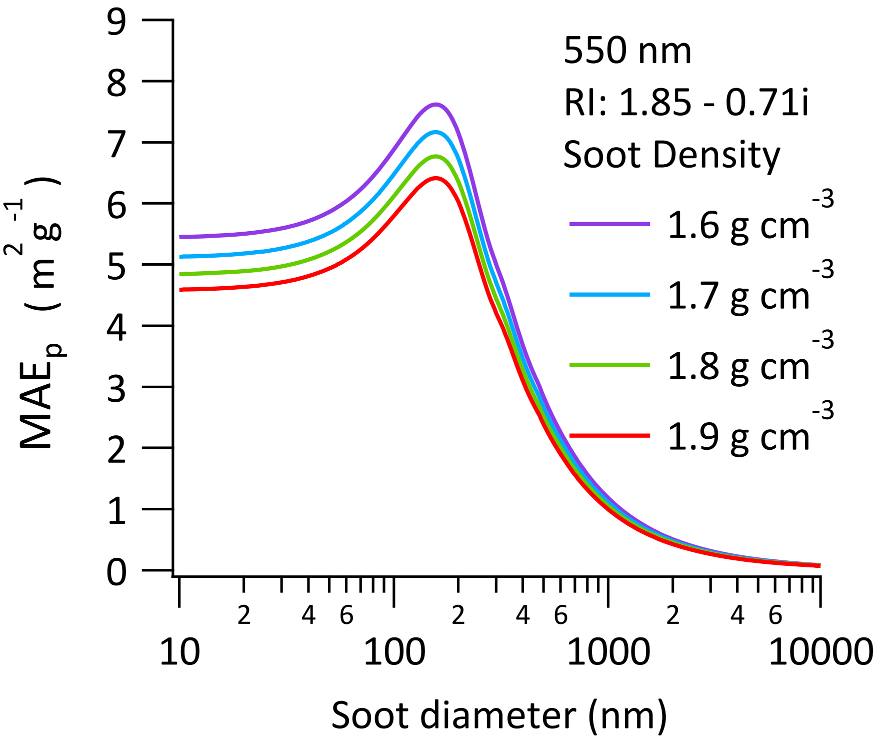

Figure S3. Mie simulated mass absorption efficiency (MAE_p) of a bare soot particle as a function of diameter at a wavelength of 550nm. Refractive index is 1.85 – 0.71i and density varied from 1.6 to 1.9 g cm^{-3}.

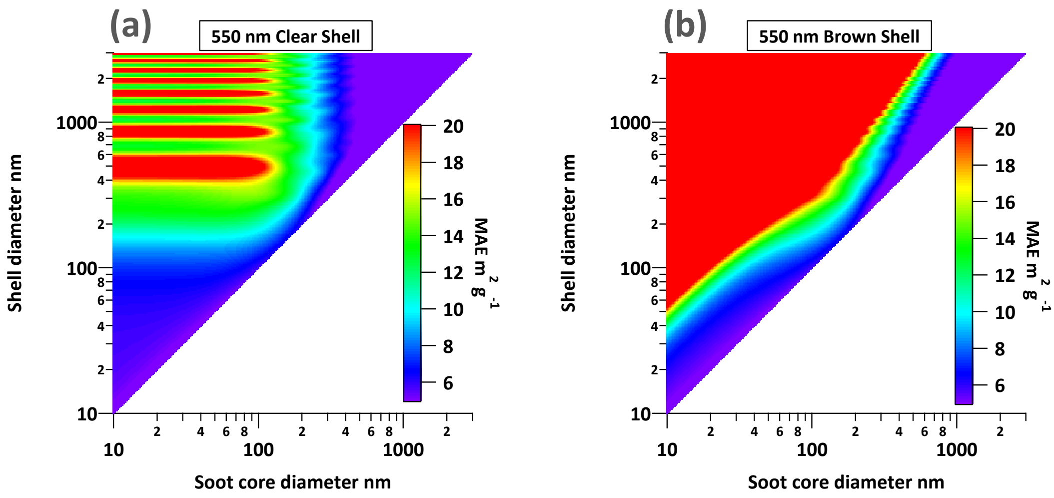

Figure S4 Mie simulated mass absorption efficiency (MAE) of a bare soot particle as a function of diameter at a wavelength of 550nm. Refractive index is 1.85 – 0.71i and density is 1.9 g cm^{-3} for soot core. Refractive index for clear coating is 1.55. Refractive index for brown coating is wavelength dependent adopted from Lack and Cappa (Lack and Cappa, 2010).

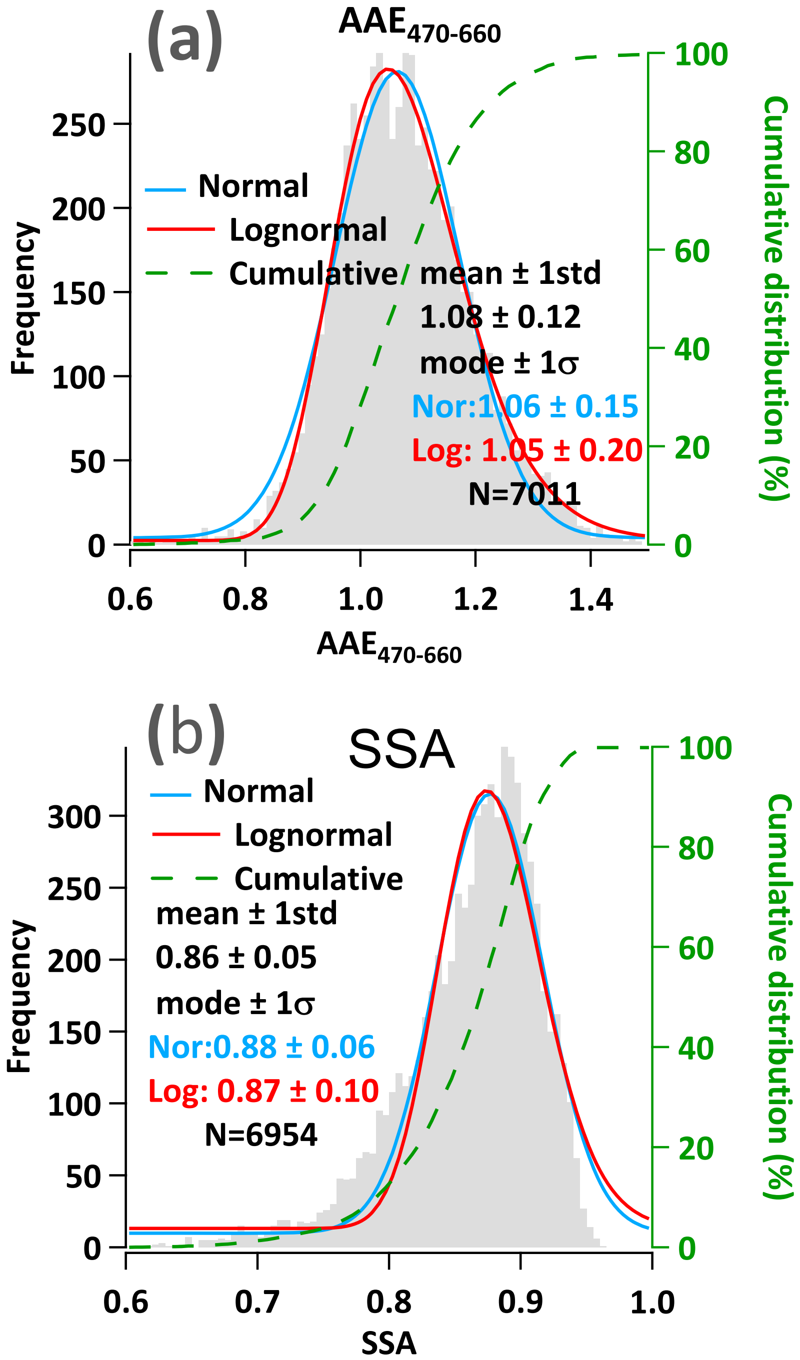

Figure S5. Measured annual statistics of AAE$_{470-660}$, and SSA. (a) Annual frequency distribution of AAE at 550 nm. (b) Annual frequency distribution of SSA. The blue and red line represent normal and lognormal fitting curve respectively.

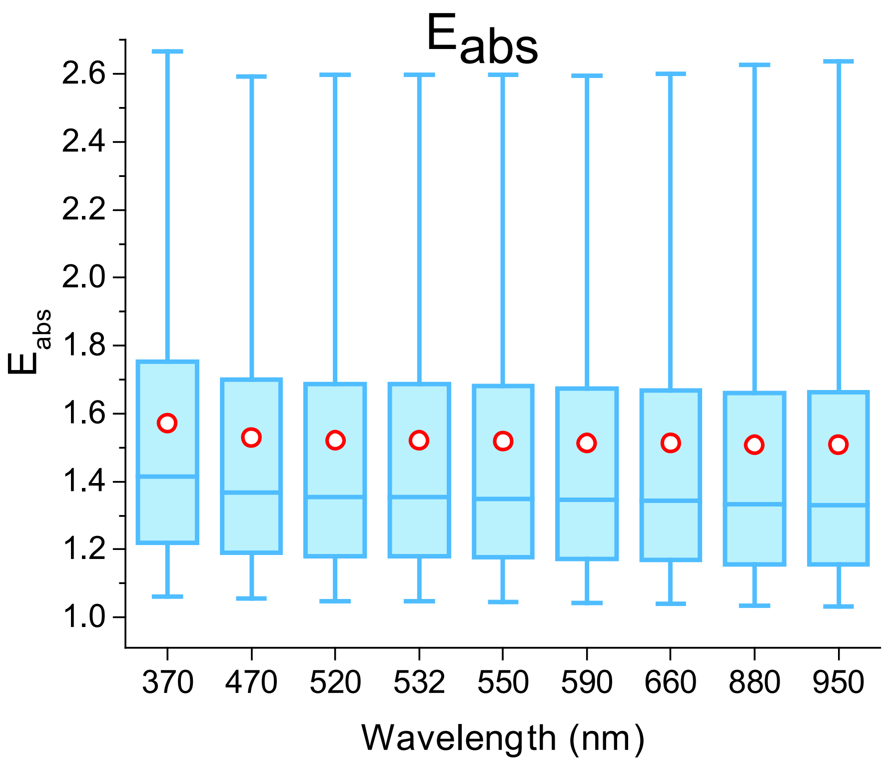

Wavelength (nm)	370	470	520	532	550	590	660	880	950
E_{abs} mean	1.57	1.53	1.52	1.52	1.52	1.51	1.51	1.51	1.51
E_{abs} S.D.	0.52	0.51	0.51	0.51	0.51	0.51	0.52	0.53	0.53

Figure S6. Spectrum annual average E_{abs} from 370 to 950 nm.

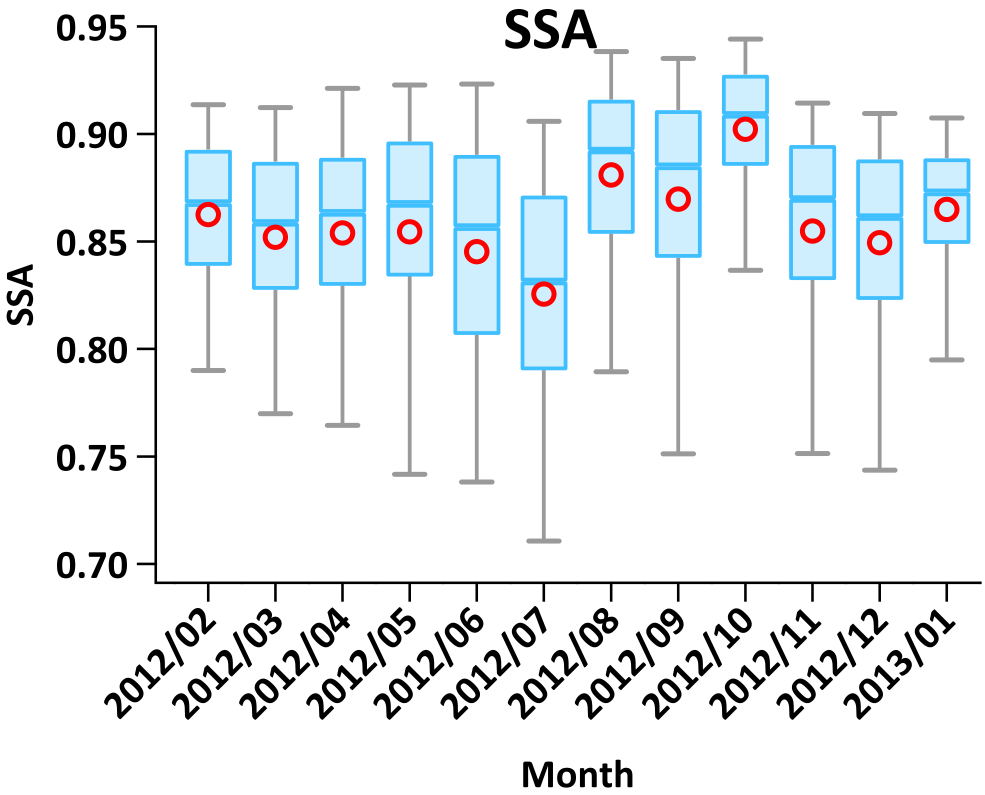

Figure S7. Measured monthly variations of SSA.

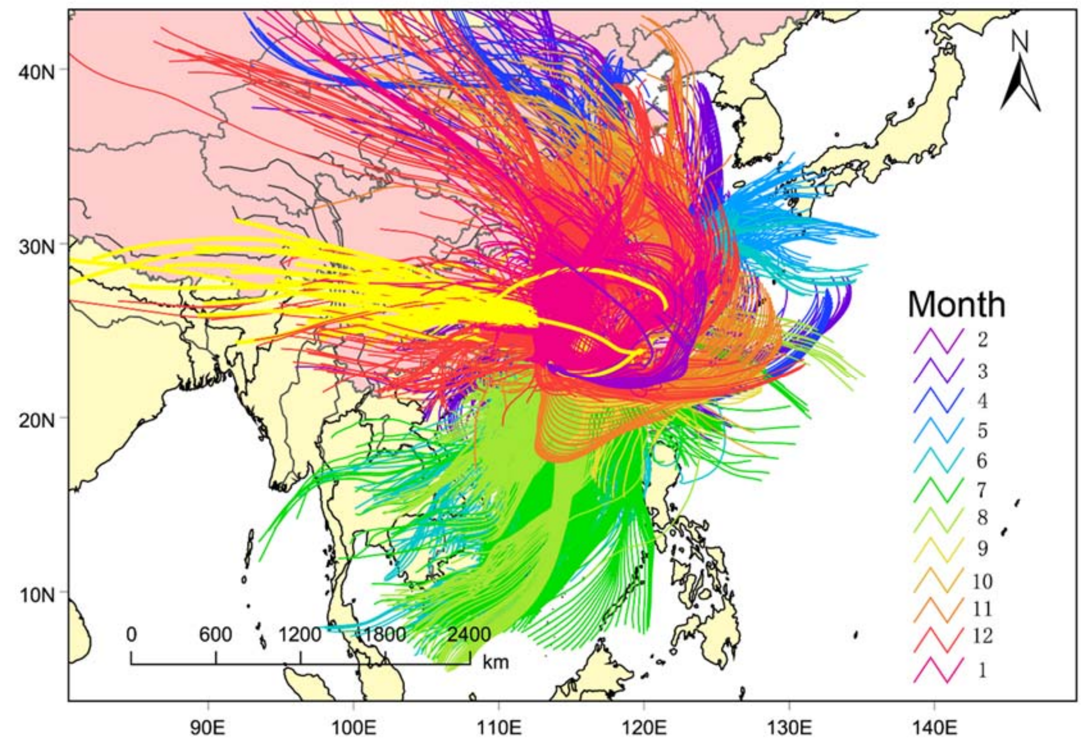

Figure S8. Hourly back trajectories for the past 72 hours calculated using NOAA's HYSPLIT model from Feb 2012 to Jan 2013. The color coding represents different months.

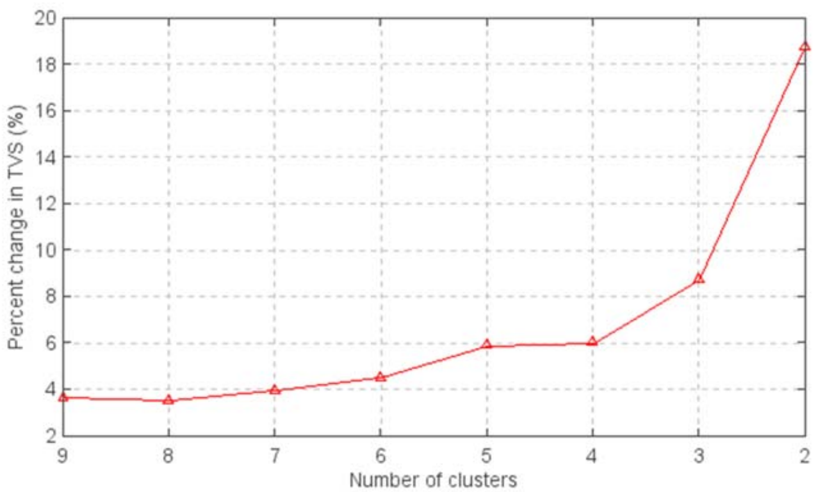

Figure S9. Total spatial variance (TSV) as a function of number of clusters in back trajectories clustering analysis.

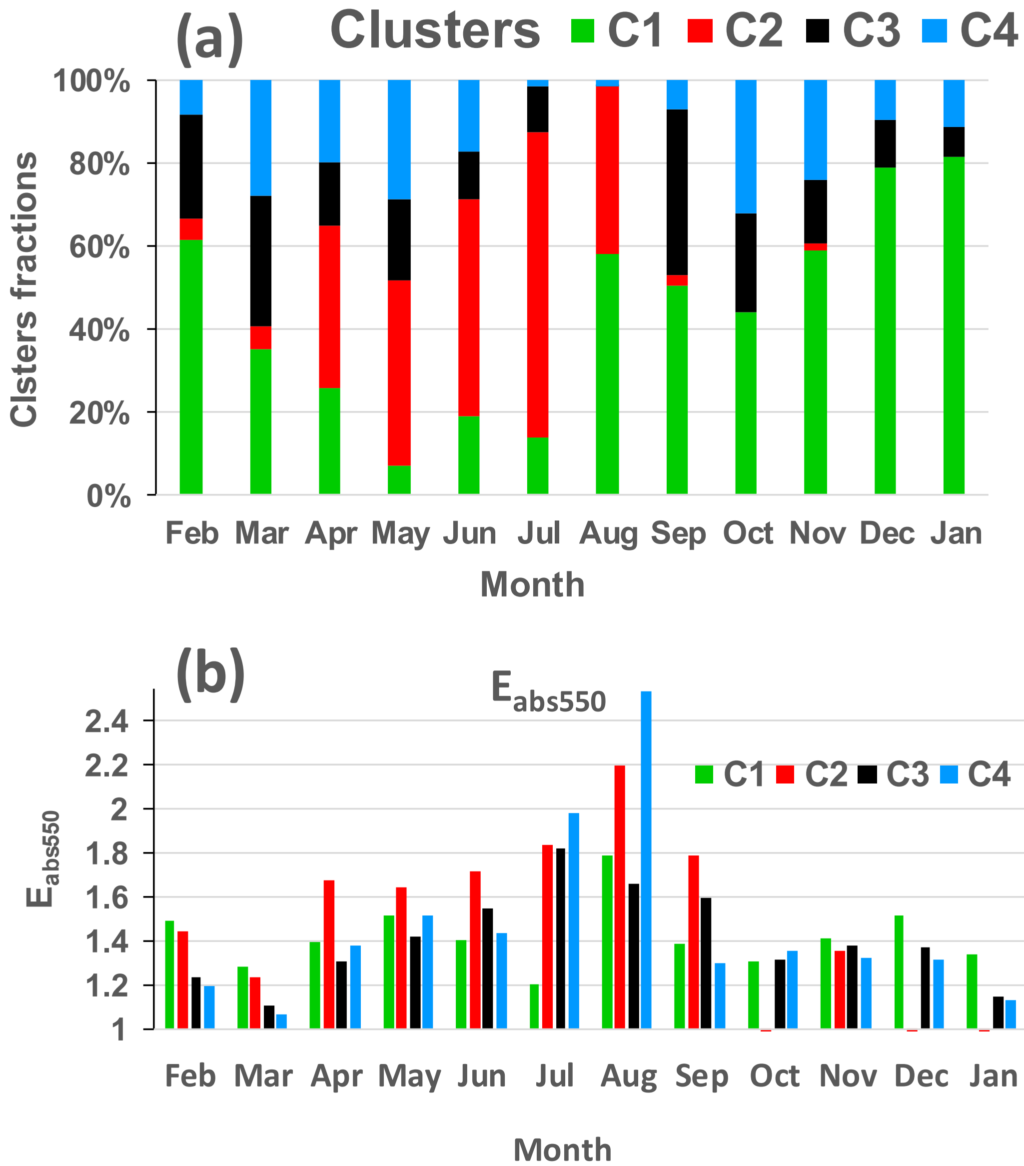

Figure S10. (a) Monthly contribution of each cluster. (b) Monthly E_{abs550} of each cluster.

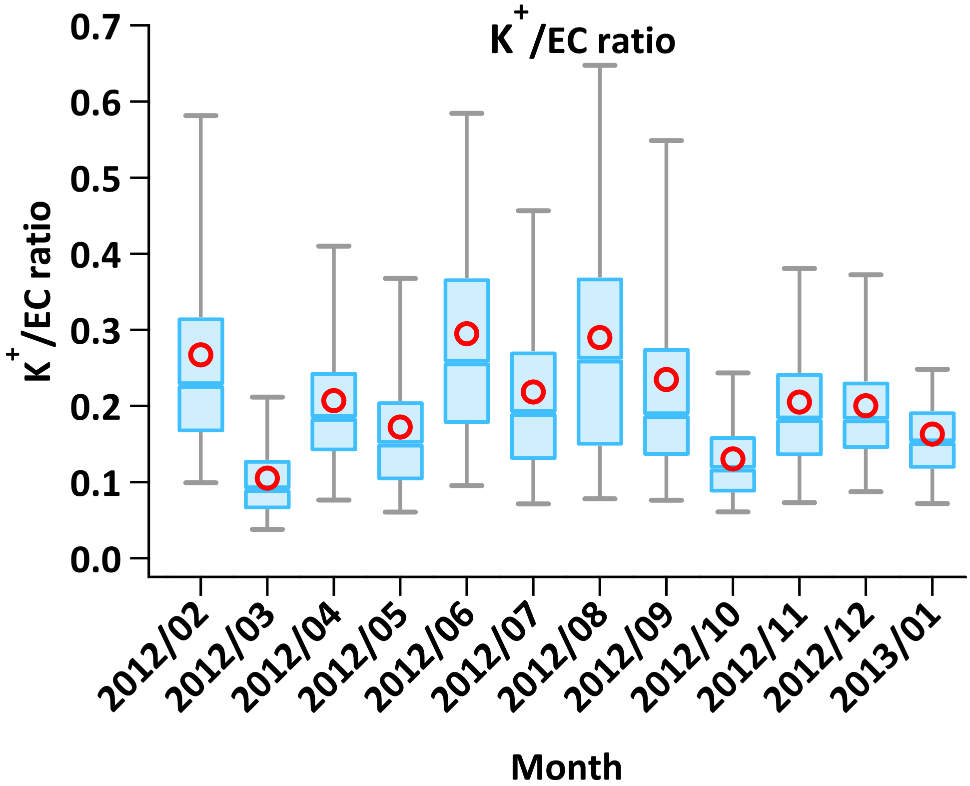

Figure S11. Monthly variations of K^+/EC ratio from 2012 Feb to 2013 Jan at NC site.

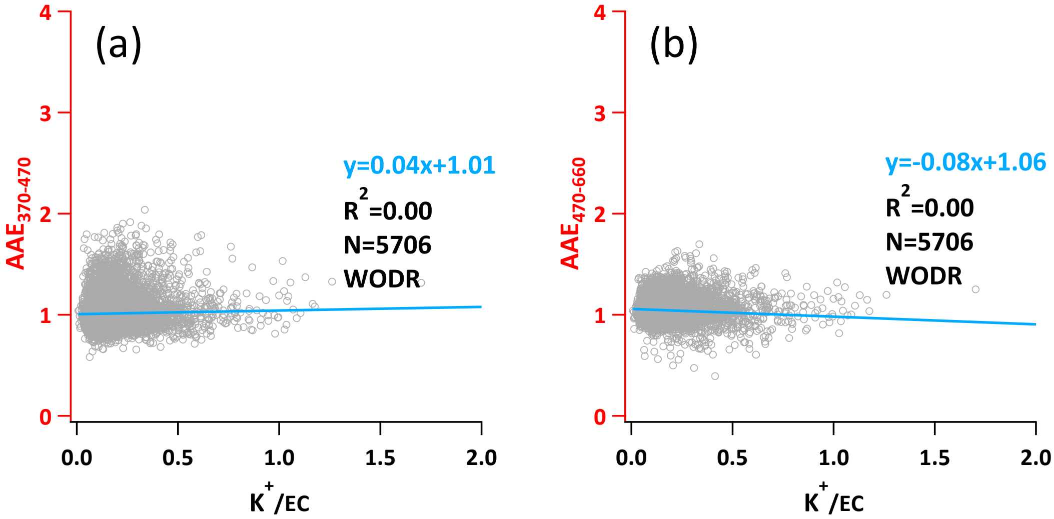

Figure S12. Correlations of AAE with K^+/EC ratio (biomass burning indicator). (a) AAE from 370 – 470 nm. (b) AAE from 470 – 660 nm.

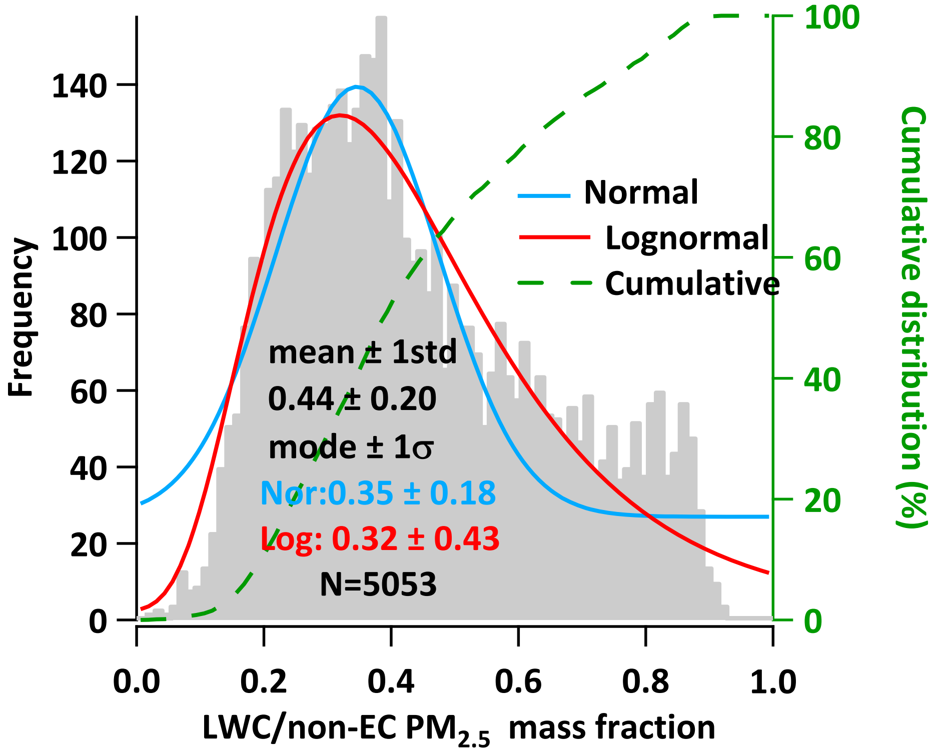

Figure S13. Annual frequency distribution of LWC/non-EC $PM_{2.5}$ mass fraction.

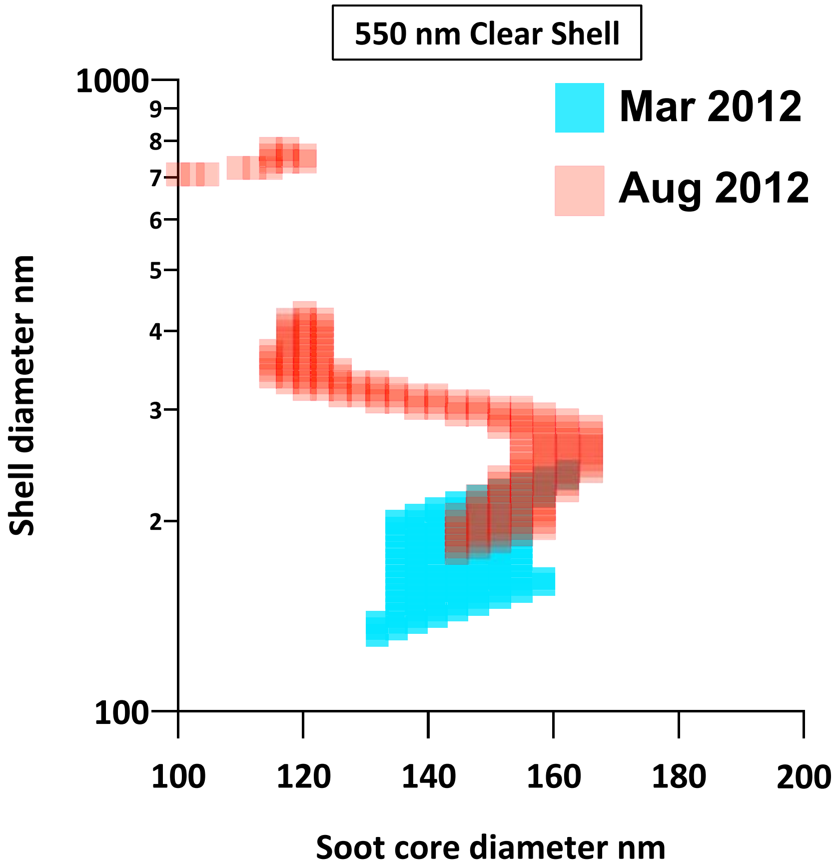

Figure S14. Size range of soot particles constrained by E_{abs} and $AAE_{470-660}$ from measurements.

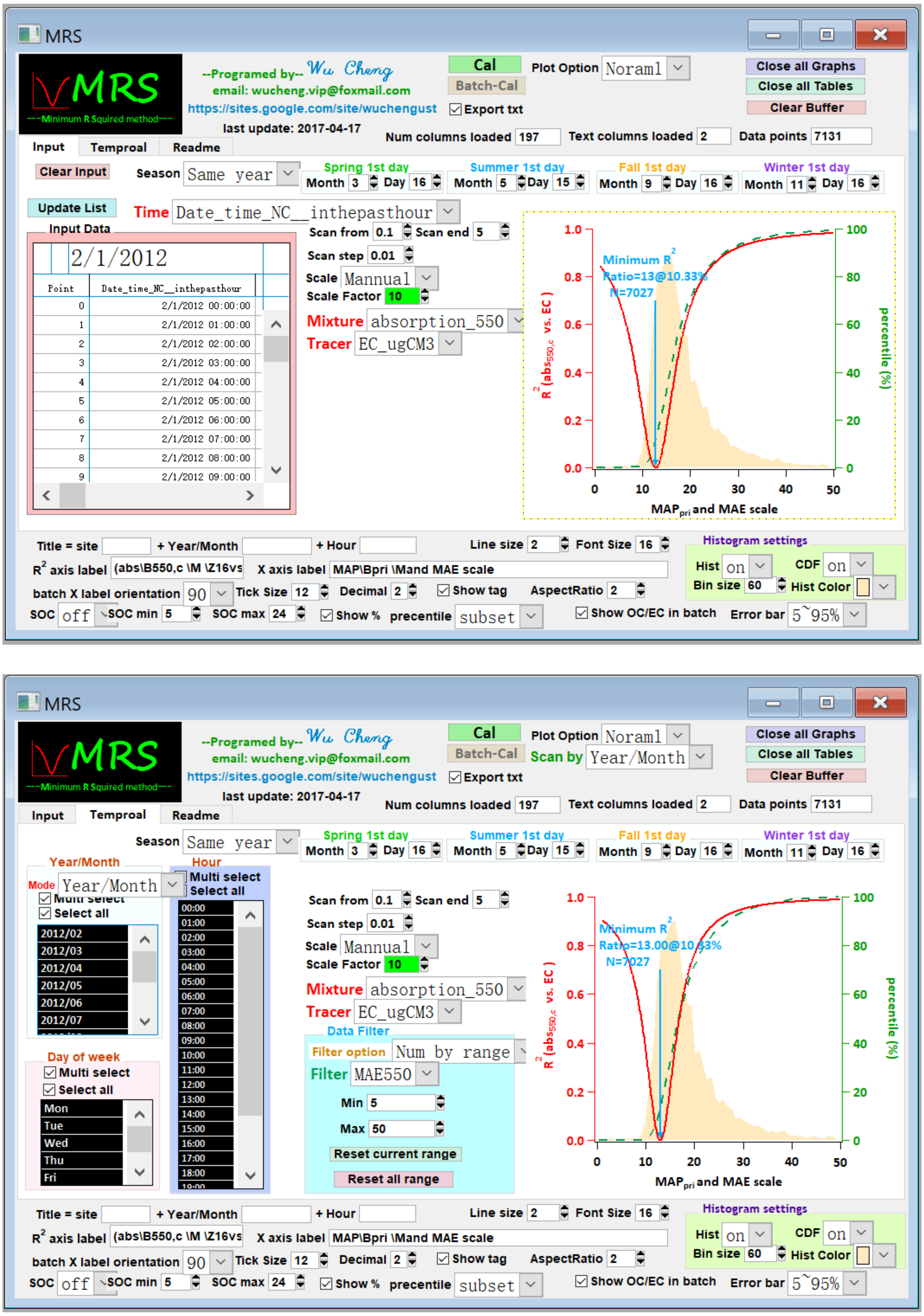

Figure S15. MRS program written in Igro Pro (WaveMetrics, Inc. Lake Oswego, OR, USA). Available from https://sites.google.com/site/wuchengust.

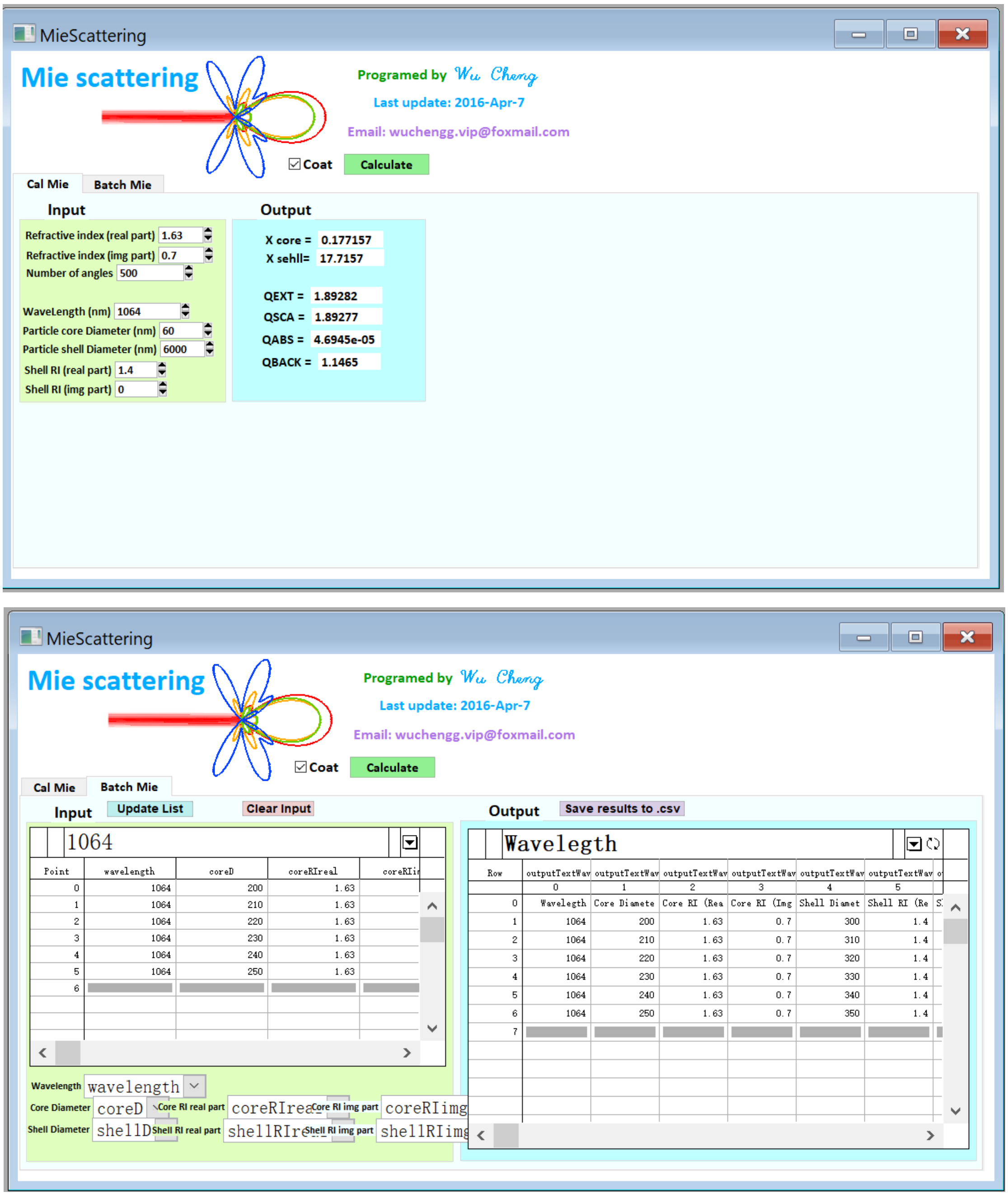

Figure S16. Mie program written in Igro Pro (WaveMetrics, Inc. Lake Oswego, OR, USA). Available from https://sites.google.com/site/wuchengust.

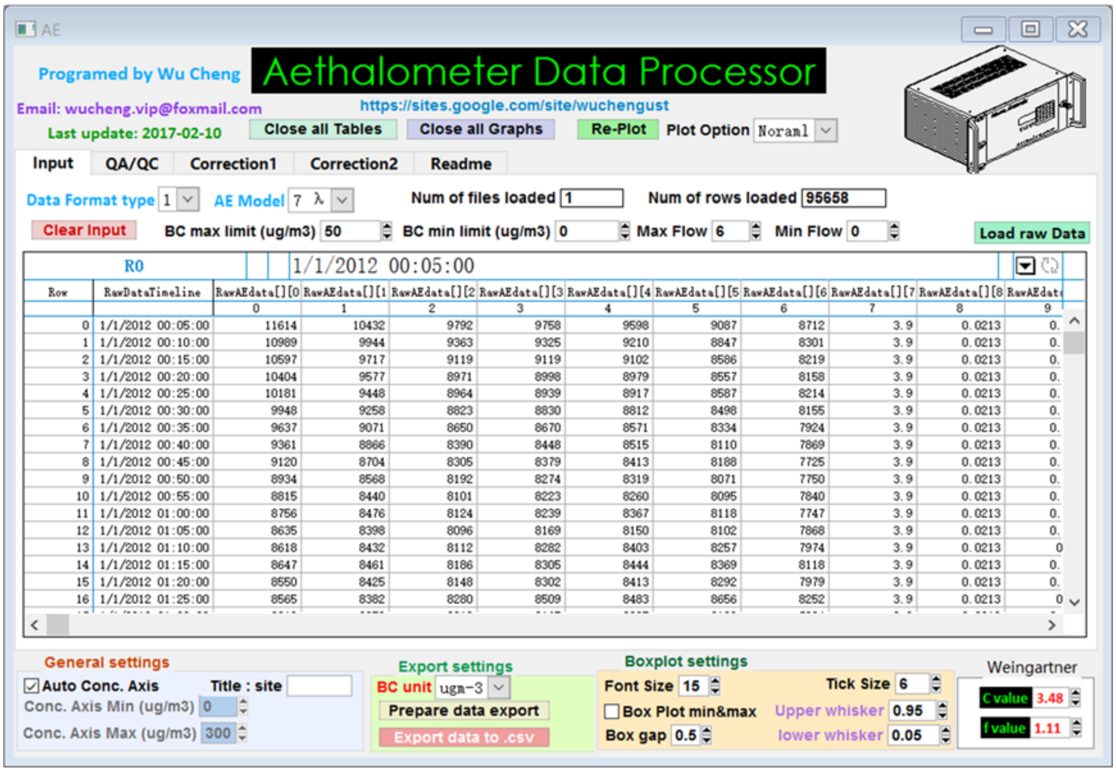

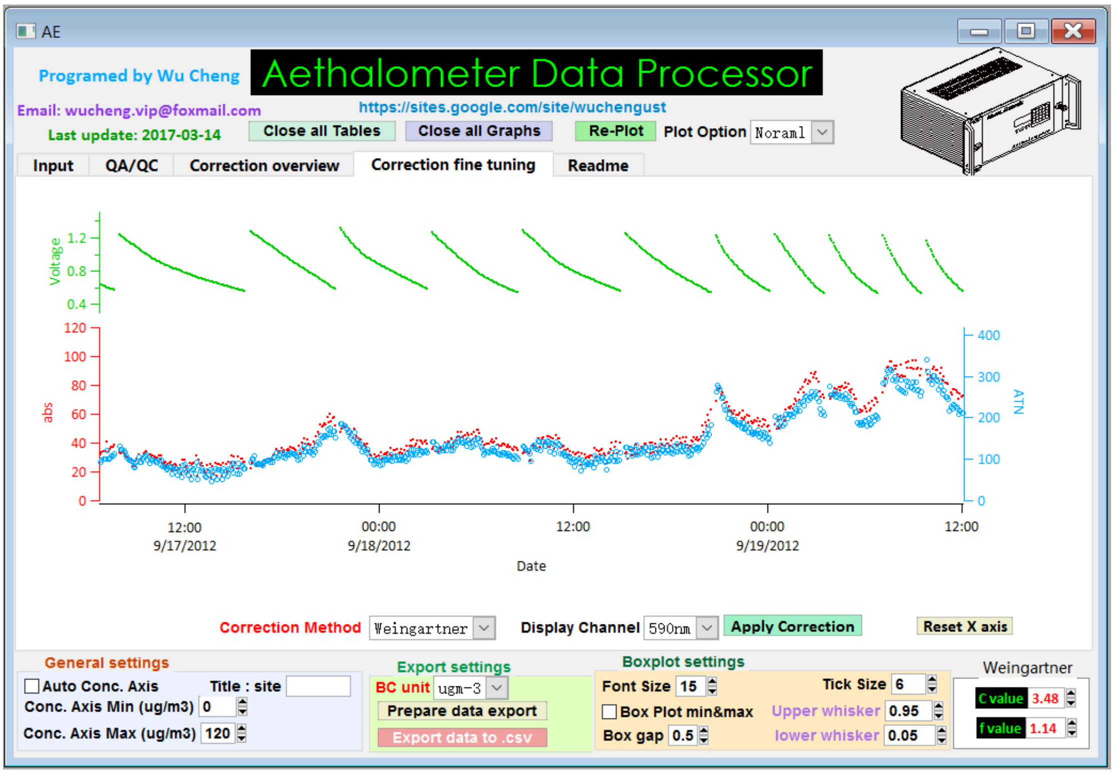

Figure S17. Aethalometer data processing program written in Igro Pro (WaveMetrics, Inc. Lake Oswego, OR, USA). Available from https://sites.google.com/site/wuchengust.

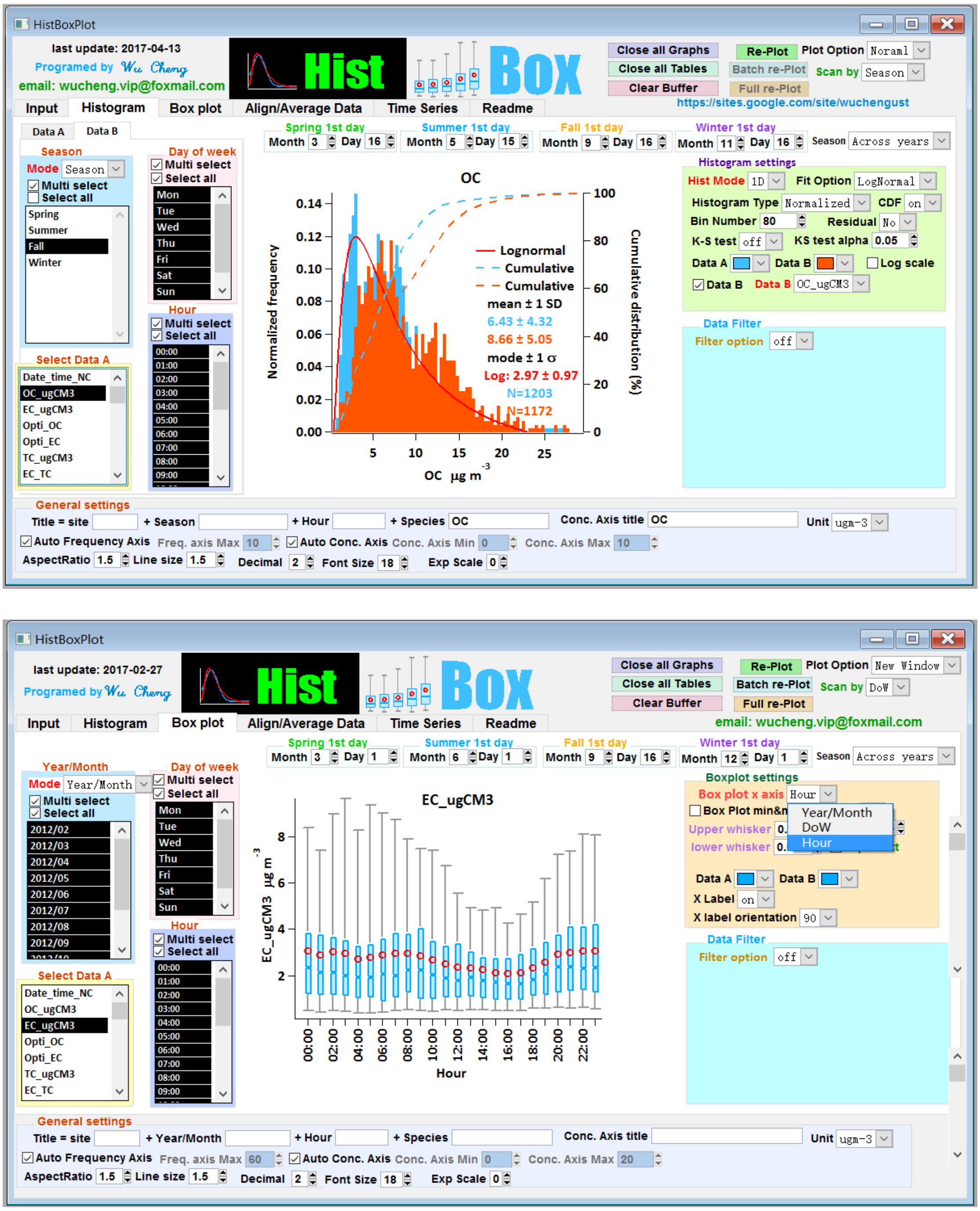

Figure S18. Histbox program written in Igro Pro (WaveMetrics, Inc. Lake Oswego, OR, USA). Available from https://sites.google.com/site/wuchengust.

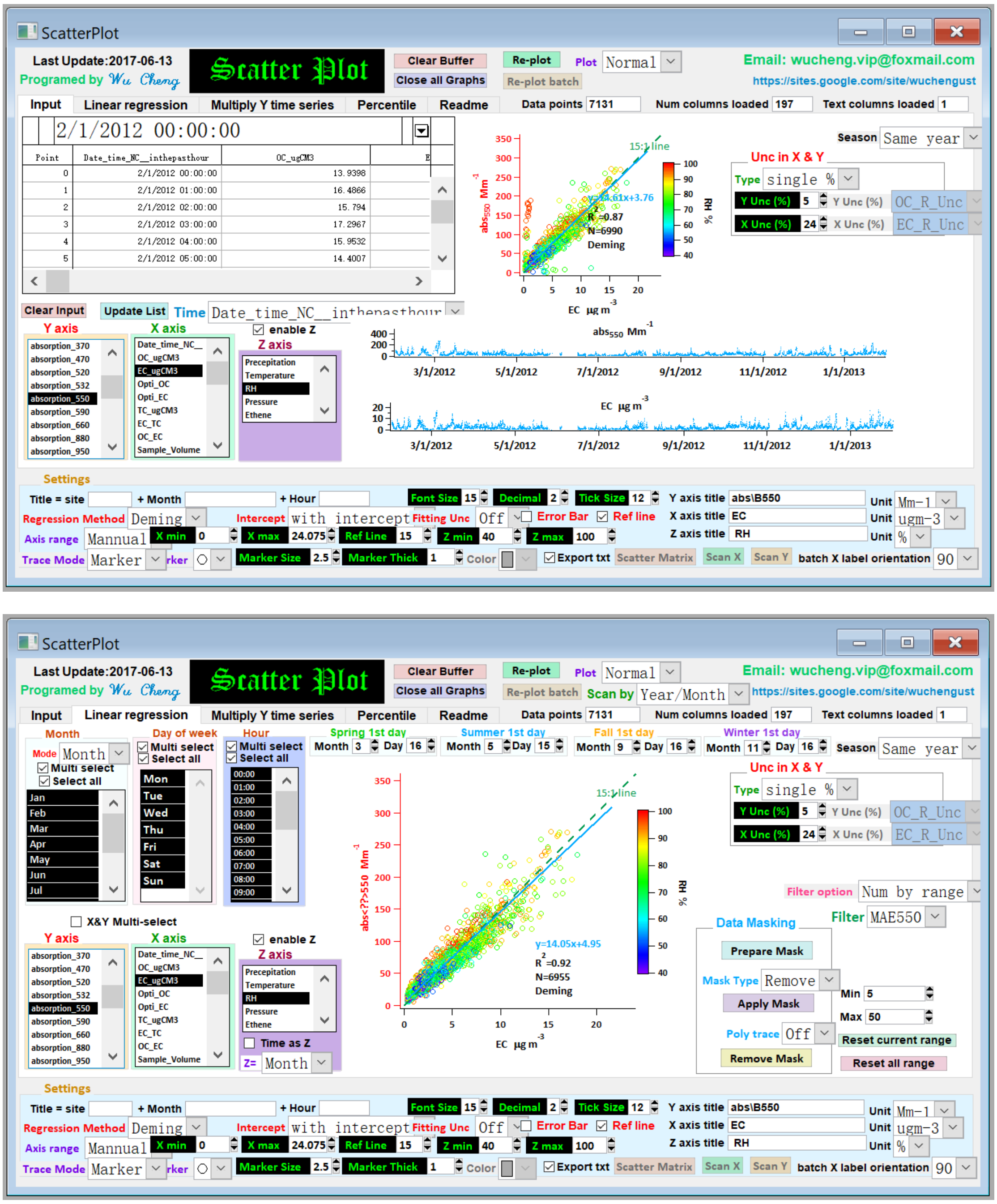

Figure S19. Scatter plot program written in Igro Pro (WaveMetrics, Inc. Lake Oswego, OR, USA). Available from https://sites.google.com/site/wuchengust.